Journal of Alloys and Compounds 504 (2010) 395–402

Contents lists available at ScienceDirect

Journal of Alloys and Compounds

journal homepage: www.elsevier.com/locate/jallcom

Electrical and magnetic behaviour of nanostructured $MgFe_2O_4$ spinel ferrite

N. Sivakumar[a,*], A. Narayanasamy[a], J.-M. Greneche[b], R. Murugaraj[c], Y.S. Lee[d]

[a] Materials Science Centre, Department of Nuclear Physics, University of Madras, Guindy Campus, Chennai 600 025, India
[b] Laboratoire de Physique de l'Etat condensé, UMR CNRS 6087, Université du Maine, Faculté des Sciences, 72085 Le Mans Cedex 9, France
[c] Department of Applied Sciences and Humanities, Madras Institute of Technology, Anna University, Chennai 600 044, India
[d] Faculty of Applied Chemical Engineering, Chonnam National University, 300 Yongbong-dong, Gwang-ju 500-757, Republic of Korea

ARTICLE INFO

Article history:
Received 11 November 2009
Received in revised form 18 May 2010
Accepted 28 May 2010
Available online 8 June 2010

PACS:
72.20.–I
75.50.Pp
73.63.–b
73.63.Bd
77.22.Gm

Keywords:
Nanostructured $MgFe_2O_4$
High-energy ball milling
Cation distribution
Electrical behaviour
Mössbauer spectroscopy

ABSTRACT

Nanostructured $MgFe_2O_4$ spinel has been synthesized with various grain sizes ranging from 72 to 19 nm using ceramic method and followed by high-energy ball milling. The observed electrical conductivity decreases with grain size is mainly due to the size effect than the cation distribution which is clearly evident by in-field Mössbauer measurement. The saturation magnetization of the 72 nm grain size sample has been enhanced and it is about 39% larger than that of their bulk (micron size particle). The observed increase in the coercivity of the milled sample is due to the smaller crystalline size, increase in the grain boundary volume and also due to surface anisotropy of increasing number of ions on the surface.

1. Introduction

Nanoparticles of spinel ferrites are potential candidates in the field of magnetic and electronic applications. They have wide applications in drug delivery systems and in medical diagnostics [1]. Spinel ferrites have high electrical resistivities and low dielectric losses which are useful in microwave devices, computer memories and magnetic recording. Among the spinel ferrites family, magnesium ferrite is a soft magnetic n-type semiconducting material [2], which finds a number of applications in sensor technology, thermal coagulation therapy, in which tumors are locally heated by application of alternating magnetic fields [3]. The structural formula of $MgFe_2O_4$ is generally written as $(Mg_{1-\lambda}Fe_{\lambda})[Mg_{\lambda}Fe_{2-\lambda}]O_4$, where parentheses and square brackets indicate cation site of tetrahedral (A) and octahedral [B] coordination, respectively, and where λ represents the degree of inversion defined as a fraction of (A) sites occupied by Fe^{3+} ions.

In recent years, nanosized milled spinel ferrites exhibit interesting magnetic and electrical properties which are different from those of the bulk counterparts. The variation of the Néel temperature with grain size [4,5], a high coercivity [6] and enhanced magnetic moments [7,8] has been observed in nanosized ferrite particles compared with those of bulk samples. The Néel temperature of $Ni_{0.5}Zn_{0.5}Fe_2O_4$ spinel ferrite was shown to increase from 538 K in the bulk state to 611 K when the grain size was reduced to 14 nm using high-energy ball milling [9]. In the past five decades, impedance spectroscopy is used to investigate the dynamics of bound and/or free ions in the bulk or in the interfacial regions of any kind of solid or liquid materials such as ionic, semiconducting, mixed electronic–ionic and dielectrics. The dispersion in conductivity has been seen in a broad variety of disordered solids like, amorphous semiconductors, ionic and electronic conducting polymers, ion conducting glasses, highly defective crystals or doped semiconductors and single crystals [10–14]. Ponpandian et al. [15] have reported that the real part of dielectric constant (ε') and dielectric loss ($\tan\delta$) for milled samples are about two orders of magnitude smaller than those of bulk in the case of $NiFe_2O_4$.

Several reports are available in the literature on the magnetic properties of nanoscale $MgFe_2O_4$ [16–22]. A few investigators have studied the electrical properties in the case of bulk $MgFe_2O_4$

* Corresponding author. Present address: Faculty of Applied Chemical Engineering, Chonnam National University, 300 Yongbong-dong, Gwang-ju 500-757, Republic of Korea. Tel.: +82 62 530 1904; fax: +82 62 530 1909.
E-mail address: nskdnp@gmail.com (N. Sivakumar).

0925-8388/$ – see front matter © 2010 Elsevier B.V. All rights reserved.
doi:10.1016/j.jallcom.2010.05.125

[23–25]. This has motivated us to carry out electrical conductivity and dielectric measurements on nanostructured $MgFe_2O_4$. In order to explain the results obtained from the electrical conductivity and dielectric measurements, we have also performed in-field Mössbauer spectroscopy and magnetization measurements. We have, therefore, studied the effect of grain size, temperature and frequency on the electrical and magnetic properties of $MgFe_2O_4$ spinel prepared using the ceramic route and followed by high-energy ball milling.

2. Experiment

2.1. Sample preparation

The bulk $MgFe_2O_4$ spinel ferrite has been synthesized using the ceramic method. Stoichiometry mixtures of powdered reactants containing α-Fe_2O_3 and MgO were thoroughly mixed in the atomic ratio 1:1. The mixed sample was calcined at 1173 K in air and kept at this temperature for 5 h, which was furnace cooled to room temperature (300 K). The cold ferrite powder was then thoroughly ground in an agate mortar and pelletized. The pellet was then sintered at 1573 K for 5 h. The pellets were reduced to powders using agate mortar and taken to be the as-prepared sample. The as-prepared sample was milled for 10 and 15 h using planetary high-energy ball mill (Fritsch pulverisette 7) with zirconia vials and balls. The milling speed of vials and balls was 300 rpm with a ball to powder weight ratio of 8:1.

2.2. Sample characterization

The phase analysis for the as-prepared and milled samples was carried out using X-ray diffraction (XRD) with a Rigaku-make high precision Guinier X-ray diffractometer and Fe Kα radiation. The average grain size was determined from the full-width at half-maximum of the (3 1 1) reflection of the XRD patterns using Scherrer's formula [26]. Surface morphological features of the as-prepared and milled samples were observed using a field emission scanning electron microscope (FE-SEM, S-4700, Hitachi, Japan).

2.3. Electrical and magnetic measurements

The electrical conductivity and dielectric measurements were done using an impedance analyzer (Solatron 1260 Impedance/Gain-Phase Analyzer) in the temperature range from 300 to 550 K and in the frequency range from 1 Hz to 10 MHz. The powder was made into a pellet by applying a pressure of 50 MPa for these measurements and the sample was sandwiched between two platinum electrodes. In order to homogenize the charge carriers and to remove the moisture content, the pellet was preheated up to 423 K for 30 min, before starting the measurements. The real (Z') and imaginary (Z'') parts of the complex impedance (Z^*) were measured as a function of both frequency and temperature. The temperature of the sample was measured with a resolution of $\pm$1 K using a Eurotherm (818 P) PID temperature controller, the heating rate being 2 K/min. The conductivity (σ), the real (ε') part of dielectric constant and dielectric loss, $\tan\delta$ were calculated using the raw data of Z' and Z'' and the sample dimensions.

Magnetic measurements were made using a vibrating sample magnetometer (Model: EG&G PARC 4500, USA) (VSM). The ^{57}Fe Mössbauer spectra were recorded at 10 K under a magnetic field of 8 T applied parallel to the γ-ray direction. The degree of inversion was calculated from the subspectral areas ($I_{(A)}/I_{[B]} = f_{(A)}/f_{[B]} \times x/(2-x)$), assuming that the ratio of the recoilless fractions is $f_{(A)}/f_{[B]} = 1$ at low temperatures [27].

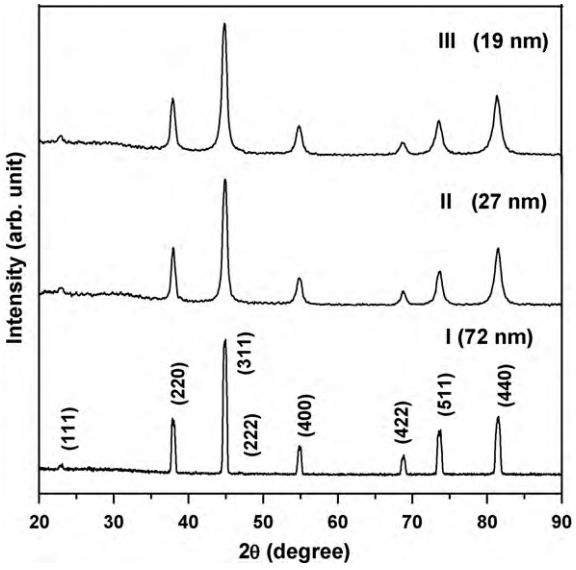

Fig. 1. The XRD patterns of $MgFe_2O_4$ spinel samples: (I) as-prepared, (II) 10 h milled, and (III) 15 h milled.

3. Results and discussion

3.1. Structural analysis and surface morphology

Fig. 1 shows the X-ray diffraction patterns of the as-prepared (sample I), the 10 h milled (sample II) and the 15 h milled (sample III). The increase in the broadening of the X-ray diffraction lines gives a clear evidence for the decrease of the mean size of the milled sample. The average grain size has been calculated using Scherrer's formula by taking into account the instrumental line broadening. The average grain sizes were found to be 72, 27 and 19 nm for samples I, II and III, respectively. The microstructure of $MgFe_2O_4$ for as-prepared, 10 and 15 h milled samples are shown in Fig. 2(I), (II) and (III), respectively. The particle size of as-prepared (I) is found to lie in the range 12–23 μm. In the case of 10 h (II) and 15 h milled (III) samples, the particles are around 280–340 nm and 220–260 nm, respectively.

3.2. Electrical behaviour

3.2.1. Dc conductivity and its dependence on grain size

Fig. 3 shows the Arrhenius plot for the electrical conductivity of samples I–III in the temperature range from 370 to 500 K. The resistance was obtained by analyzing the impedance data using the non-linear least-squares (NLLS) fitting routine. The variation in conductivity with the inverse temperature is almost linear in all cases. The conductivity is found to increase with temperature for all samples, which is expected from the semiconducting behaviour of spinel ferrites, as observed earlier [9,15]. $MgFe_2O_4$ is reported to be an n-type semiconductor [2], due to the hopping of electrons from Fe^{2+} to Fe^{3+} ions in the octahedral [B] sites. The activation energy for the electrical conductivity is obtained from the Arrhenius relation,

$$\sigma T = \sigma_0 \exp\left[-\frac{E_a}{k_B T}\right] \quad (1)$$

where σ_0 is the pre-exponential factor with the dimensions of ($\Omega\,cm^{-1}$)K, E_a is the activation energy for dc conductivity and k_B is the Boltzmann constant. Table 1 shows the values of activation energies obtained for samples I–III. We have observed that the activation energy increases with the grain size reduction, which reflects the blocking nature of grain boundary [10]. The blocking nature of the grain–grain contacts was suggested to be due to the seg-

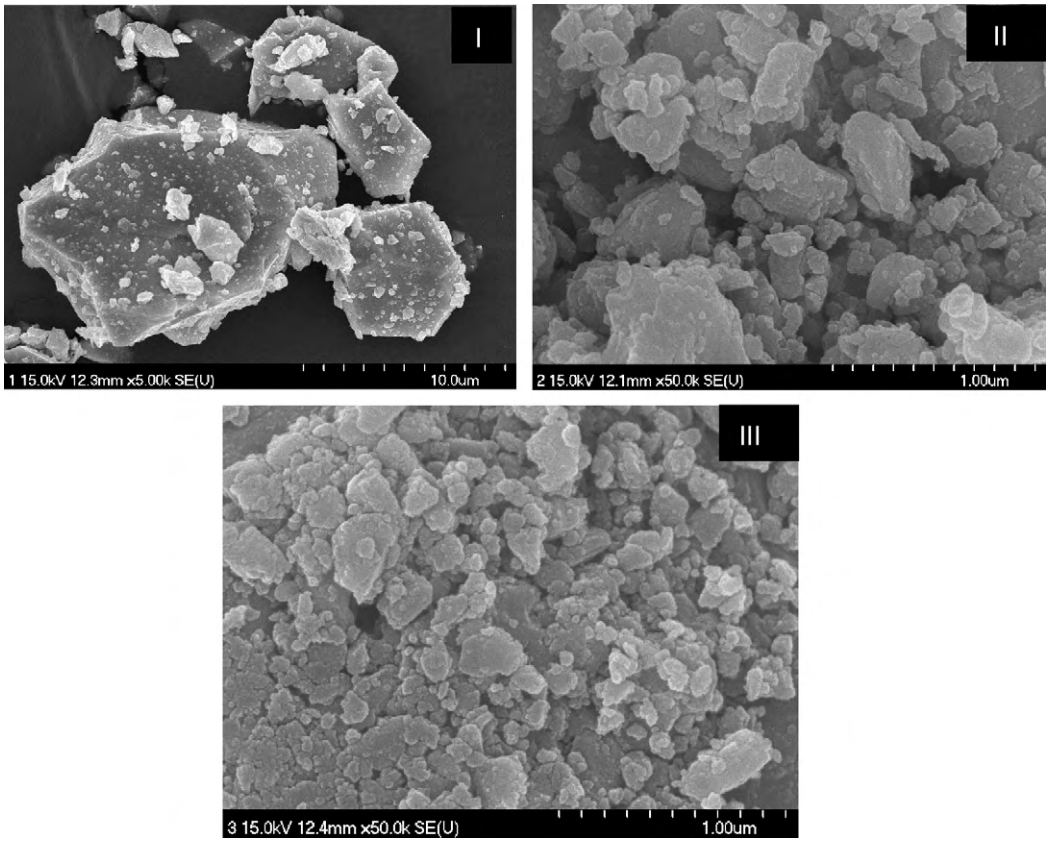

Fig. 2. The SEM images of $MgFe_2O_4$ spinel samples: (I) as-prepared, (II) 10 h milled, and (III) 15 h milled.

regation of host lattice cations, lattice mismatching, dislocations, defects, etc. As seen from Fig. 3, the conductivity decreases with the reduction of grain size by high-energy milling. Normally, conductivity depends on the combined influence of several factors such as Fe^{2+} ion concentration, grain size, crystal structure perfection and microstructural homogeneity. In general, the conductivity in ferrites arises mainly from the electron hopping between the Fe^{2+} and Fe^{3+} ions present on equivalent lattice sites (octahedral site) [28]. The distance between the cations in A-sites is larger than the distance between cations in B-sites, and moreover the degree of covalency for the A-site ions is known to be higher than that of the B-site cations [15]. Due to the structural difference and the higher degree of covalency in A-sites, the mobility of electrons and holes in the A-sites is expected to be smaller than that in the B-sites. The present in-field Mössbauer studies clearly show that the Fe^{3+} ion concentration increases in octahedral site [B-site] for the milled samples (Section 3.3). Therefore, we expect that the conductivity should increase upon milling, but, we have observed a contradicting behaviour. The decrease in conductivity with grain size reduction, therefore, can be attributed to the size effects as reported in the literature [29,30] and also due to the increase in grain boundary volume and the associated impedance to the flow of charge carriers. If the crystallite size is smaller than the electron mean free path, then the grain boundary scattering becomes dominant, and therefore, the electrical resistivity is expected to increase. The low conductivity samples have reduced eddy current losses at high frequencies, and therefore, the milled ferrite samples in the present study are suitable for high frequency applications.

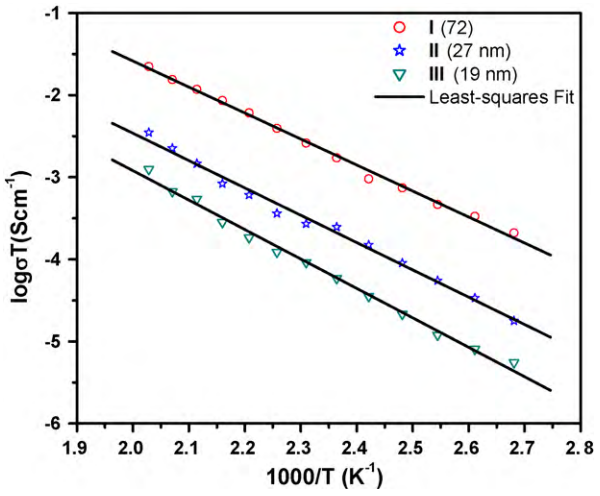

Fig. 3. The Arrhenius plots for the electrical conductivity of nanocrystalline $MgFe_2O_4$ spinel samples. The solid lines are the least-squares fit to Eq. (1).

3.2.2. Dielectric behaviour

The frequency dependence of the real part of dielectric constant (ε') and dielectric loss factor ($\tan\delta$) at 300 K for all grain sizes is shown in Fig. 4(a and b), respectively. From Fig. 4(a), it is observed that the ε' initially increases, then decreases gradually with respect

Table 1
The values of activation energies for electrical conductivity in $MgFe_2O_4$ spinel ferrite samples. E_a is the activation energy obtained from the conductivity data.

Sample (grain size in nm)	Activation energy for the electrical conductivity E_a (eV) [±0.01]
I (72)	0.62
II (27)	0.65
III (19)	0.69

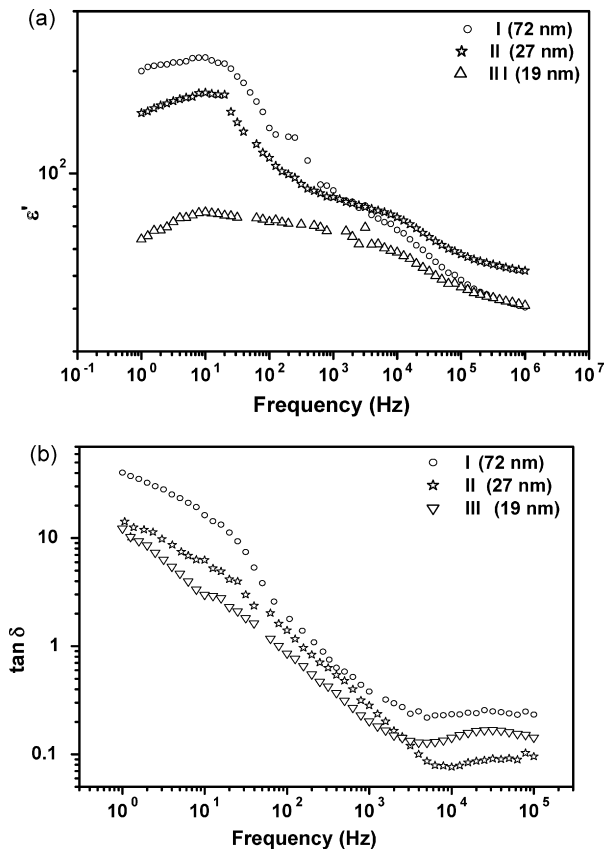

Fig. 4. (a) The real part of the dielectric constant (ε') at 300 K as a function of frequency for different grain sizes of $MgFe_2O_4$ sample. (b) The dielectric loss factor ($\tan\delta$) at 300 K as a function of frequency for different grain sizes of $MgFe_2O_4$ sample.

to frequency for all the samples (I–III). In general, the dielectric constant is mainly contributed by the atomic and electronic polarizations in ferrite grains. In normal behaviour, ε' decreases with frequency because the electron hopping between $Fe^{2+} \leftrightarrow Fe^{3+}$ ions cannot follow the ac field beyond a certain frequency. In the case of $MgFe_2O_4$, the presence of Mg^{2+} ions gives rise to p-type carriers in addition to the n-type carriers arising from the electron exchange between Fe^{2+} and Fe^{3+} ions [31]. The anomalous dielectric behaviour can be explained as being due to a collective contribution of the n- and p-type carriers to the polarization. The local displacements of p-type carriers in the direction of the external electric field also contribute to the net polarization in addition to the n-type carriers. Moreover, the mobility of the p-type carriers is smaller than that of the n-type carriers, the contribution to the polarization from the former will decrease more rapidly and even at lower frequencies. Therefore, the net contribution will increase initially and then decrease with frequency. The position of the maximum of ε' will be dependent on the relative number of p-type carriers in the material. The higher the number of p-type carriers, the higher the peak frequency.

Rezlescu and Rezlescu [32] have observed the similar behaviour in the case of Cu–Ni ferrites. In the present studies, ε' is lower for the milled samples (II and III) compared to that of the as-prepared sample (I). The change in ε' of ferrite is mainly due to the variation in the concentration of Fe^{2+} ions. The higher the concentration of the Fe^{2+} ions, the higher the value of ε' [33,34]. Our in-field Mössbauer results (as reported in Section 3.3) clearly indicate that some of the Fe^{3+} ions have migrated from tetrahedral (A) to octahedral [B] sites for the milled samples (II and III). Therefore, we expect that the value of ε' should increase with milling for samples II and III because of the increase in the number of Fe^{3+} and Fe^{2+} pairs. But, we have observed the reverse trend which is due to the number of Mg^{2+} ions displaced from the B-sites to the A-sites increases upon milling. This will lead to a decrease in the number of magnesium ion pairs and hence the number of available p-type carriers in the B-sites. Dube [35] has also observed a decrease in dielectric constant by about 3–8% compared to bulk particles (50 μm and above). El Hiti [24] has obtained a value of 10^4 for ε' at 312 K (at 1 kHz) for the bulk $MgFe_2O_4$. In the present studies, ε' is found to be around 10^2 for the milled samples (II and III) at the same temperature and frequency, which are two orders of magnitude smaller than that of the bulk $MgFe_2O_4$.

The plot between dielectric loss ($\tan\delta$) and frequency has been shown in Fig. 4(b). The value of $\tan\delta$ decreases with frequency for all the samples, which is a normal behaviour [15]. When the jumping rate of charge carriers lags behind the ac field beyond a certain critical frequency, $\tan\delta$ decreases. The value of $\tan\delta$, is found to decrease with the reduction of grain size upon milling, which is quite similar from our previous studies on $NiFe_2O_4$ [15] and $ZnFe_2O_4$ [36]. In the case of $ZnFe_2O_4$ [36], $\tan\delta$ decreases with the reduction of grain size is mainly due to the reduction of Fe^{3+} ions in B-site upon milling. The reduction of the number of $Fe^{2+} \leftrightarrow Fe^{3+}$ ion pairs in the B-sites and therefore the polarization also decreases with the grain size reduction. Hence, the major contribution to $\tan\delta$ in ferrites comes from electron hopping between $Fe^{2+} \leftrightarrow Fe^{3+}$ ion pairs [37]. Therefore, we expect that the value of $\tan\delta$ should increase with milling for samples II and III. But, in the present studies, the decrease in $\tan\delta$ upon milling is mainly due to size effect. El Hiti [24] has obtained a value of 10^1 for $\tan\delta$ at 312 K (at 1 kHz) for the bulk $MgFe_2O_4$ ferrite prepared by ceramic method. In the present study, $\tan\delta$ for all samples is about 0.3 at 300 K and at the same frequency. The dielectric loss is thus found to be two orders of magnitude lower compared to that of the bulk [24].

3.2.3. Electrical modulus studies

Fig. 5 shows the plot between the imaginary part of modulus (M'') and frequency for sample III (19 nm) at selected temperatures. The relaxation peak for $M''(\omega)$ moves towards higher frequency with temperature. It means that the relaxation time for this process decreases with temperature. The plot between scaled M''/M''_{max} vs. $\log(f/f_{max})$ for sample III (19 nm) is shown in Fig. 6 for various temperatures, where f_{max} corresponds to the peak frequency of the M'' vs. $\log f$ plots. From Fig. 6, it is observed that all the curves for different temperatures overlap on a single master cure for sample III (19 nm) indicating that the relaxation mechanism is temperature independent. Moreover, Fig. 7 shows that the peaks of the nor-

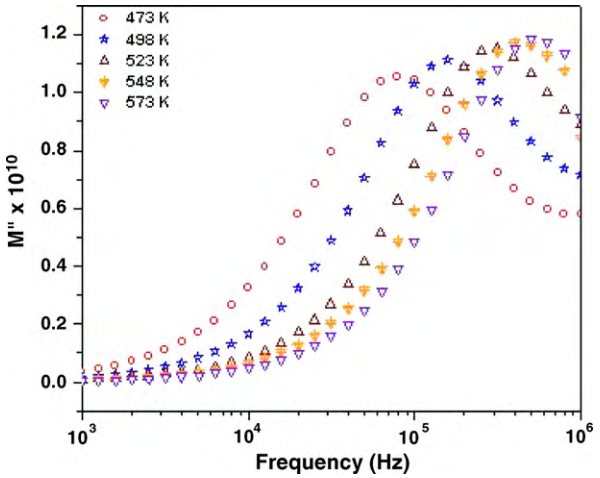

Fig. 5. The imaginary part (M'') of modulus spectra for $MgFe_2O_4$ sample with 19 nm grain size (sample III).

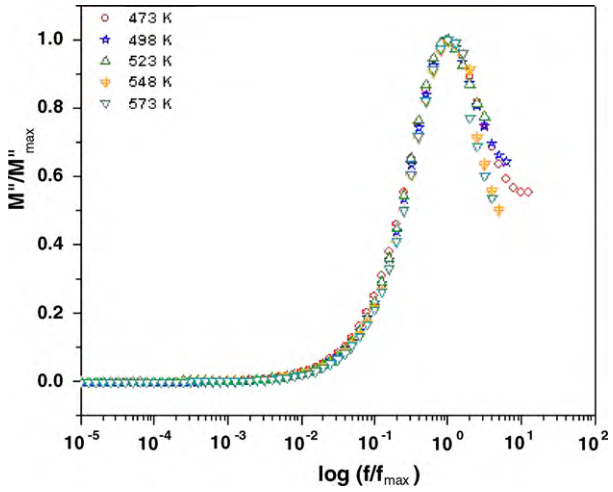

Fig. 6. The plots of M''/M''_{max} vs. $\log(f/f_{max})$ for sample III (19 nm) of $MgFe_2O_4$ spinel ferrite at various temperatures.

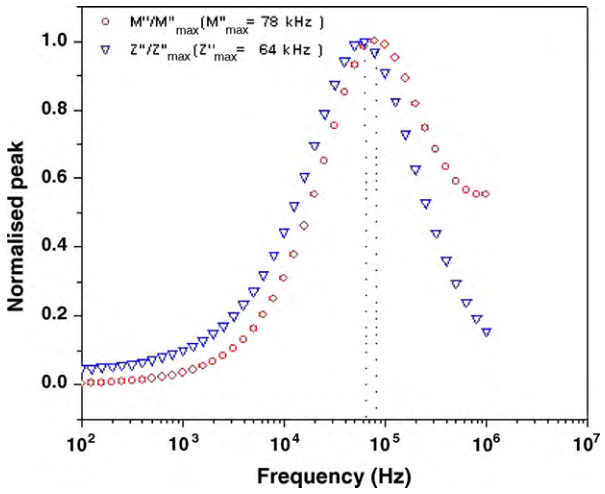

Fig. 8. The logarithmic plot of normalized parameters (M'', Z'') for sample III (19 nm) of $MgFe_2O_4$ spinel ferrite measured at 473 K.

malized M'' curves for all the grain sizes overlap on a single master curve, but in the higher frequency range there is some deviation due to grain interior effect which is nothing but the grain effect. From Fig. 6, the value of full-width at half-maximum (FWHM) is found to be greater than 1.14 decades [38] as evaluated from the normalized modulus spectrum which suggests the existence of non-Debye type of relaxation phenomena.

Fig. 8 shows the variation of scaled parameters (M''/M''_{max} and Z''/Z''_{max}) as a function of logarithmic frequency measured at 473 K for sample III (19 nm). The figure clearly shows that the peak frequency shifts towards higher frequency region as it moves from Z'' to M''. The mismatch between the peaks of these two parameters gives an evidence for the existence of two polarization (grain and grain boundary) phenomena [39]. In general, the overlapping of the two peaks is an evidence of long-range conductivity [40]. The very distinct curves of M''/M''_{max} and Z''/Z''_{max} (Fig. 8), therefore, illustrate clearly that the polarization process is due to the localised conduction of multiple carriers which gives rise to short-range conductivity. Moreover, the localized conduction of multiple carriers describes the presence of multiple relaxation processes in the material. Also, M''/M''_{max} exhibits peak value at high frequency and it reduces to zero at low frequencies. This suggests that the electrode polarization is negligible or absent.

3.2.4. The ac conductivity studies

The ac conductivity and permittivity above the dielectric loss peak frequency ($\omega > \omega_p$) are empirically and, respectively, represented as $\sigma'(\omega) \propto \omega^n$ and $\varepsilon'(\omega) \propto \omega^{n-1}$, with $0 < n \leq 1$. The ac conductivity has been measured in a wide frequency range at different temperatures. The frequency dependence of the conductivity at various temperatures is shown in Fig. 9.

Almond and West [41] have pointed out that the dispersive behaviour of the ac conductivity of certain conducting materials can be expressed as,

$$\sigma_{ac} = \sigma_{dc} + A\omega^n = \sigma_{dc}\left[1 + \left(\frac{\omega}{\omega_p}\right)^n\right] \quad (2)$$

which is called the universal power law.

The conductivity spectra for different temperatures are fitted to Eq. (2) for all samples using NLLS fitting and the parameters σ_{dc}, ω_p, and n are extracted from the analysis. The frequency exponent, n takes values near or just below unity depending on the frequency ω in the characteristic power law and the parameter A is frequency independent, but may be temperature dependent. The above equation is general and is universally found for amorphous semiconductors, glasses and electronic conductors. Many theoretical models have been developed to identify the origin of power law dispersion. The power law features are also observed with

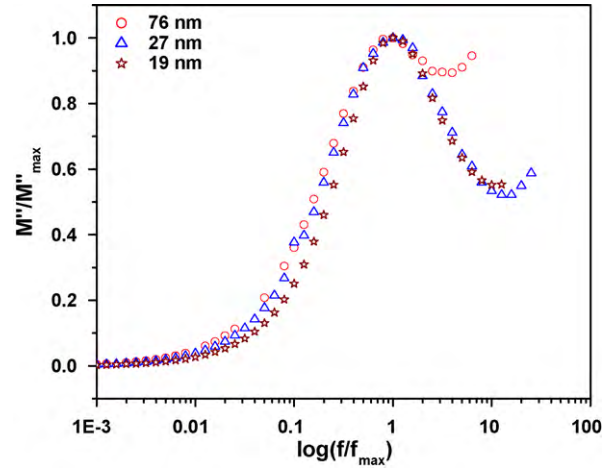

Fig. 7. The plots of M''/M''_{max} vs. $\log(f/f_{max})$ for various grain sizes of $MgFe_2O_4$ spinel ferrite measured at 473 K.

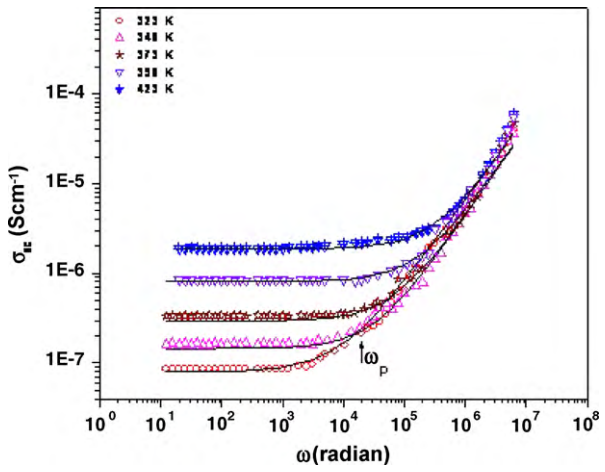

Fig. 9. The frequency dependence of the ac conductivity of sample I (72 nm) of $MgFe_2O_4$. The continuous lines are fitted with Eq. (2).

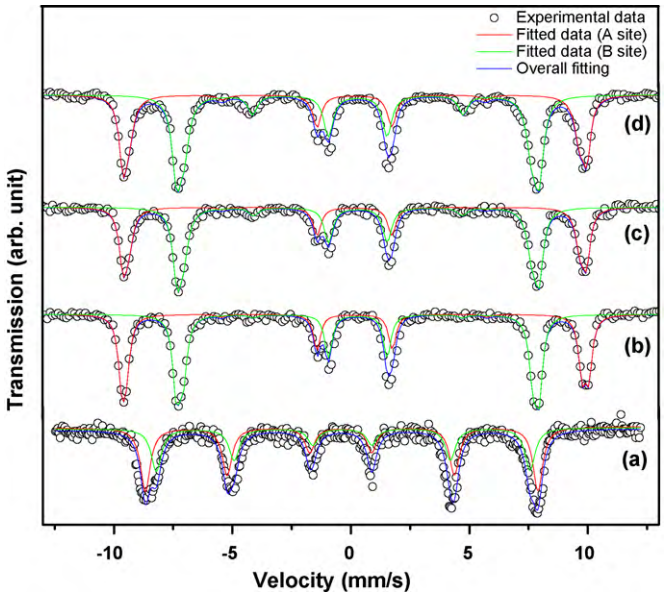

Fig. 10. Room temperature (298 K) Mössbauer spectrum of the as-prepared sample of $MgFe_2O_4$ taken in zero applied magnetic field (a), and under a magnetic field of 8 T applied parallel to the γ-ray direction taken at 10 K for (b) as-prepared: 72 nm, (c) 10 h milled: 27 nm, and (d) 15 h milled sample: 19 nm.

other non-Debye dielectric response functions such as Cole–Cole, Cole–Davidson and Havirliak–Negami [42–44].

According to Almond and West [41], the above equation can be written as,

$$\sigma_{ac} = \sigma_{dc}\left(1 + (\omega\tau)^n\right) \quad (3)$$

where τ is the relaxation time.

In the present study the frequency dependent conductivity data for sample I (72 nm) for various temperatures were fitted with the above equation as shown in Fig. 9. The frequency independent plateaus in the $\log_{10}\sigma$ vs. $\log_{10}\omega$ plots are identified with the dc conductivities of the materials. In the high frequency range, the increase of bulk conductivity is due to the high frequency dispersion. We have observed, from Fig. 9, such frequency independent plateau repeatedly over several decades of frequency for all the measured temperature ranges. But the increase in conductivity is limited to higher frequencies by an additional grain interior effect [45]. This takes the form of a power law increase in conductivity with the frequency.

3.3. Mössbauer studies

Mössbauer spectrum of the as-prepared (sample I) $MgFe_2O_4$ taken at 300 K in zero applied magnetic field (Fig. 10(a)) indicates that there is a partial overlap of the (A) and [B] subspectra because of the small difference in the hyperfine fields of the Fe^{3+} ions in the two sublattices. But, in the presence of an external magnetic field, the effective particle moment is aligned to the applied field with some degree; the resulting magnetic field at iron nucleus is either increased or decreased by the applied field depending upon the direction of alignment of the magnetic moments relative to the applied magnetic field. Therefore, we have recorded the 8 T Mössbauer spectra for the as-prepared (sample I) and milled (samples II and III) $MgFe_2O_4$ at 10 K and are shown in Fig. 10. The Mössbauer spectra were fitted with two magnetic components arising from the tetrahedral (A) and octahedral site (B) Fe^{3+} ions. The experimental data have been fitted using the least-squares MOSFIT program. The degree of inversion is found to be $x = 0.880(4)$ for sample A, which indicates that the sample is a partly inverse spinel with the Néel type collinear spin arrangement $(Mg_{0.12}Fe_{0.88}\uparrow)[Mg_{0.88}Fe_{1.12}\downarrow]O_4$. Moreover, for the milled samples the degree of inversion are $x = 0.819$ (9) and $x = 0.780$ (0) for samples II and III, respectively (see Table 2). The observation is that the milling process decreases the fraction of Fe^{3+} ions on (A) sites. The site occupancy of the milled samples (II and III) may be written as $(Mg_{0.18}Fe_{0.82}\uparrow)[Mg_{0.82}Fe_{1.18}\downarrow]O_4$ and $(Mg_{0.22}Fe_{0.78}\uparrow)[Mg_{0.78}Fe_{1.22}\downarrow]O_4$, respectively. Many reports are available to clearly show that high-energy milling is able to induce redistribution of cations between (A) and [B] sites [11,46,47]. The presence of the 2nd and 5th lines of Mössbauer sextet in an external field applied parallel to the direction of γ-rays is because of the canting of the Fe^{3+} spins with respect to the applied field direction. The calculated average canting angles for the octahedral sites, from the altered subspectral area ratio $I_{2,5}/I_{1,6}$, were found to be $\beta_B \sim 14^\circ$, 21°, and 28° for samples I, II, and III, respectively. The canting angle β_B increases with milling. Similar behaviour has been observed [47,48] for nanocrystalline $NiFe_2O_4$; they conclude that spin canting may be due to the surface effects where the spins on the surface layer are canting. Moreover, Kodama et al. [49] have reported that $NiFe_2O_4$ fine particles coated with organic surfactant have ferrimagnetically aligned core spins and a spin-glass-like surface layer. They have also proposed that the surface spin disorder in ferrimagnetic spinel nanoparticles is due to the broken exchange bonds in the near-surface layers. The increase in canting angle with decreasing grain size is due to the increase in the percentage of Mg^{2+} ions occupying A-sites and increase in the surface area as the grain size decreases with milling. The increase in the concentration of Mg^{2+} ions in A-sites will result in the decrease in the number of nearest neighbour magnetic ions to the B-site Fe^{3+} ion and hence the canting angle increases with milling.

3.4. Magnetization studies

Magnetization hysteresis curves measured at 298 and 77 K for the as-prepared (sample I) and 15 h milled (sample III) $MgFe_2O_4$ using VSM are shown in Fig. 11. The saturation magnetization for sample I (72 nm) was found to be 36 and 42 emu/g (magnetic moment μ is 36 emu/g, as calculated from in-field Mössbauer

Table 2
Mössbauer parameters: isomer shift $\langle IS\rangle$, quadrupole shift $\langle 2\varepsilon\rangle$, effective hyperfine field $\langle B_{eff}\rangle$ (algebraic sum of the internal hyperfine magnetic field and the external applied magnetic field), hyperfine field $\langle B_{hyp}\rangle$ canting angle $\langle\gamma\rangle$, and relative intensity of the sextets $\langle I_{ref}\rangle$ for the $MgFe_2O_4$ samples at 10 K in an external magnetic field of 8 T applied parallel to the direction of γ-rays.

Sample (grain size in nm)	Fe site	$\langle IS\rangle$[a] (mm/s) ±0.01	$\langle 2\varepsilon\rangle$ (mm/s) ±0.02	$\langle B_{eff}\rangle$ (T) ±0.5	$\langle B_{hyp}\rangle$ (T) ±0.5	$\langle\gamma\rangle$ (°) ± 5	$\langle I_{ref}\rangle$ (%) ±1
I (72)	A	0.34	0.00	60.2	52.4	12	44
	B	0.47	0.00	46.5	54.3	14	56
II (27)	A	0.33	0.00	59.8	52.4	12	41
	B	0.48	0.00	46.5	54.0	21	59
III (19)	A	0.33	−0.00	59.8	52.0	12	39
	B	0.48	−0.03	46.5	53.6	28	61

[a]With respect to α-Fe at 300 K.

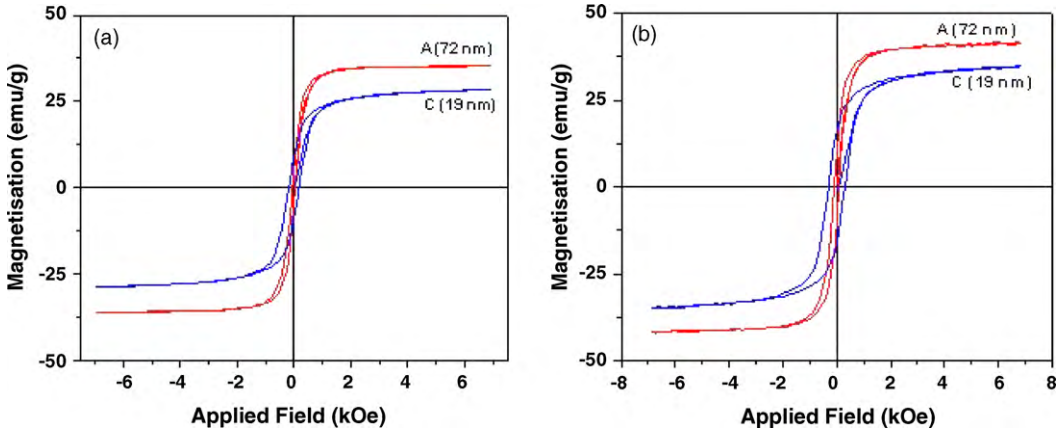

Fig. 11. The magnetization hysteresis loops for as-prepared and 15 h milled samples of $MgFe_2O_4$ measured at (a) 298 K and (b) 10 K.

parameters: Table 2) at 298 and 77 K, respectively, whereas in the case of bulk it is only 27 and 31 emu/g (magnetic moment μ from Mössbauer is 31 emu/g) at 293 and 0 K [extrapolated to 0 K], respectively [28]. The cation distribution of the bulk $MgFe_2O_4$ is $(Mg_{0.1}Fe_{0.9}\uparrow)[Mg_{0.9}Fe_{1.1}\downarrow]O_4$. Šepelák et al. [20] have observed the saturation magnetization to be 37 emu/g measured at 3 K for $MgFe_2O_4$ with 10 nm grain size prepared by mechanosynthesis route. From the in-field Mössbauer studies, they have estimated the cation distribution as $(Mg_{0.24}Fe_{0.76}\uparrow)[Mg_{0.76}Fe_{1.14}\downarrow]O_4$ (the effective magnetic moment, μ is 67 emu/g). Therefore, our observation is that the saturation magnetization of the 72 nm grain size sample (I) [the cation distribution is $(Mg_{0.22}Fe_{0.78}\uparrow)[Mg_{0.78}Fe_{1.22}\downarrow]O_4$] is enhanced by about 33% than that of its bulk [the cation distribution is $(Mg_{0.1}Fe_{0.9}\uparrow)[Mg_{0.9}Fe_{1.1}\downarrow]O_4$ [28] because of the change in the cation distribution. Moreover, another observation is that the milling process leads to reduction of magnetization for sample III (Fig. 10). The value of saturation magnetization as obtained from VSM measurements is found to be 28 and 34 emu/g at 298 and 77 K, respectively. As per the cation distribution (Table 2), the saturation magnetization should increase upon milling. The value calculated from the cation distribution for sample III is 44 emu/g. But, the observed reverse trend is because of the existence of non-magnetic surface layer caused by the canting of surface spins or a high anisotropy layer or loss of the long-range order in the surface layer in the case of sample III due to the smaller grain size [50].

At 77 K the coercive field increased from 82 to 302 Oe for samples I and III, respectively. The higher coercivity of the milled sample is because of the smaller crystallite size, increase in the grain boundary volume and the structural disorder upon milling. Moreover, the increase of the surface anisotropy of small crystallites also contributes to the increase in coercivity. Chinnasamy et al. [50] have observed a similar enhancement of the coercivity for the milled nanocrystalline $NiFe_2O_4$.

4. Conclusion

The nanocrystalline $MgFe_2O_4$ samples with various grain sizes have been synthesized by ceramic route followed by mechanical milling. The conductivity is found to decrease with the reduction of grain size and also it has been observed that the activation energy for conduction increases with grain size reduction, which reflects the blocking nature of the grain boundary. The real part of the dielectric constant (ε') is found to be around 10^2 for the milled samples (27 and 19 nm grain size), which is two orders of magnitude smaller than that of the bulk $MgFe_2O_4$. The anomalous behaviour of ε', observed in the samples, has been explained based on the presence of both n- and p-type charge carriers. Moreover, the dielectric loss ($\tan\delta$) is found to be two orders of magnitude lower compared to that of the bulk $MgFe_2O_4$. The normalized modulus spectra suggest the existence of non-Debye type of relaxation phenomena for all grain sizes. The saturation magnetization of the 72 nm grain sized sample has been enhanced by about 33% compared to that of the bulk (micron sized particles).

Acknowledgement

The financial support from DST, Government of India (Sanction No. SR/S5/NM-23/2002), is acknowledged.

References

[1] Q.A. Pankhrust, J. Connolly, S.K. Jones, J. Dobson, J. Phys. D: Appl. Phys. 36 (2003) R167.
[2] R.J. Willey, P. Noirclerc, G. Busca, Chem. Eng. Commun. 123 (1993) 1.
[3] K. Konishi, T. Maehara, T. Kamimori, H. Aono, T. Naohara, H. Kikkawa, Y. Watanabe, K. Kawachi, J. Magn. Magn. Mater. 272–276 (2004) 2428.
[4] C.N. Chinnasamy, A. Narayanasamy, N. Ponpandian, R. Justin Joseyphus, B. Jeyadevan, K. Tohji, J. Magn. Magn. Mater. 238 (2002) 281.
[5] V. Šepelák, D. Schultze, F. Krumeich, U. Steinike, K.D. Becker, Solid State Ionics 141–142 (2001) 677.
[6] Y. Shi, J. Ding, J. Appl. Phys. 90 (2001) 4078.
[7] S.A. Oliver, V.G. Harris, H.H. Hamdeh, J.C. Ho, Appl. Phys. Lett. 76 (2000) 2761.
[8] J.Z. Jiang, G.F. Goya, H.R. Rechenberg, J. Phys.: Condens. Mater. 11 (1999) 4063.
[9] N. Sivakumar, A. Narayanasamy, N. Ponpandian, J.-M. Greneche, K. Shinoda, B. Jeyadevan, K. Tohji, J. Phys. D: Appl. Phys. 39 (2006) 4688.
[10] J.C. Dyre, T.B. Schrøder, Rev. Mod. Phys. 72 (2000) 873.
[11] D.L. Sidebottom, B. Roling, K. Funke, Phys. Rev. B 63 (2001) 5068.
[12] J.R. MacDonald, J. Non-Cryst. Solids 210 (1997) 70.
[13] B. Roling, Solid State Ionics 105 (1998) 185.
[14] W.K. Lee, J.F. Liu, A.S. Nowick, Phys. Rev. Lett. 67 (1991) 1559.
[15] N. Ponpandian, P. Balaya, A. Narayanasamy, J. Phys.: Condens. Mater. 14 (2002) 3221.
[16] V. Šepelák, D. Baabe, F.J. Litterst, K.D. Becker, J. Appl. Phys. 88 (2000) 5884.
[17] V. Šepelák, A. Feldhoff, P. Heitjans, F. Krumeich, D. Menzel, F.J. Litterst, I. Bergmann, K.D. Becker, Chem. Mater. 18 (2006) 3057.
[18] Z. Qi Chen, John Zhang, Appl. Phys. Lett. 73 (1998) 3156.
[19] V. Šepelák, M. Menzel, K.D. Becker, F. Krumeich, J. Phys. Chem. B 106 (2002) 6672.
[20] V. Šepelák, D. Baabe, D. Mienert, F.J. Litterst, K.D. Becker, Scr. Mater. 48 (2003) 961.
[21] S.K. Pradhan, S. Bid, M. Gateshki, V. Petkov, Mater. Chem. Phys. 92 (2005) 224.
[22] I. Bergmann, V. Šepelák, K.D. Becker, Solid State Ionics 177 (2006) 1865.
[23] D. Ravinder, K. Latha, Mater. Lett. 41 (1999) 247.
[24] M.A. El Hiti, J. Magn. Magn. Mater. 192 (1999) 305.
[25] K. Hirota, Y. Takano, M. Yoshinaka, O. Yamaguchi, Mater. Res. Bull. 35 (2005) 1137.
[26] B.D. Cullity, Elements of X-ray Diffraction, Addison Wesley, California, 1978.
[27] G.A. Sawatzky, F. Van Der Woude, A.H. Morrish, Phys. Rev. 183 (1969) 383.
[28] J. Smit, H.P.J. Wijn, Ferrites, Eindhovan, Philips, 1959.
[29] Y.Z. Wang, G.W. Qiao, X.D. Liu, B.Z. Ding, Z.Q. Hu, Mater. Lett. 17 (1993) 152.
[30] X.D. Liu, B.Z. Ding, Z.Q. Hu, K. Lu, Y.Z. Wang, Phys. B 192 (1993) 345.
[31] R.F.G. Gardner, R.L. Moss, D.W. Tanner, Brit. J. Appl. Phys. 17 (1996) 550.
[32] N. Rezlescu, E. Rezlescu, Phys. Status Solidi A 59 (1974) 575.
[33] J.T.S. Irvine, A. Huanosta, R. Velenzuela, A.R. West, J. Am. Ceram. Soc. 73 (1990) 729.

[34] C.G. Koops, Phys. Rev. 83 (1951) 121.
[35] D.C. Dube, J. Phys. D: Appl. Phys. 3 (1970) 1648.
[36] N. Ponpandian, A. Narayanasamy, J. Appl. Phys. 92 (2002) 2770.
[37] L.G. Van Uitert, Proc. IRE 44 (1956) 1294.
[38] C.T. Moynihan, L.P. Boesch, N.L. Laberge, Phys. Chem. Glass 14 (1973) 122.
[39] K. Prasad, K. Lily, K.L. Kumari, Yadav, J. Phys. Chem. Solids 68 (2007) 1508.
[40] M.A.L. Nobre, S. Lanfredi, J. Phys. Chem. Solids 64 (2003) 2457.
[41] D.P. Almond, A.R. West, Solid State Ionics 9–10 (1983) 277.
[42] D.W. Davidson, R.H. Cole, J. Chem. Phys. 19 (1951) 1484.
[43] S. Havriliak, S. Negami, Polymer 8 (1967) 161.
[44] R.H. Cole, Cole, J. Chem. Phys. 9 (1941) 341.
[45] D.P. Almond, Solid State Ionics 8 (1983) 159.
[46] S.A. Oliver, V.G. Harris, H.H. Hamdesh, J.C. Ho, Appl. Phys. Lett. 76 (2000) 2761.
[47] A.H. Morrish, K. Haneda, J. Appl. Phys. 52 (1981) 2496.
[48] A.H. Morrish, K. Haneda, P.J. Schiurer, J. Phys. C 6 (1976) 301.
[49] R.H. Kodama, A.E. Berkowitz, E.J. McNiff, S. Foner, J. Appl. Phys. 81 (1997) 5552.
[50] C.N. Chinnasamy, A. Narayanasamy, N. Ponpandian, R. Justin Joseyphus, B. Jeyadevan, K. Tohji, K. Chattopahyay, J. Magn. Magn. Mater. 238 (2002) 281.